LSST #395737, VOL 44, ISS 9

Buoyancy-Driven Continuous SPLITT Fractionation: A New Technique for Separation of Microspheres

Jonathan Storey, Phil Douglas, Phil Ligrani, and Karl Morten

QUERY SHEET

This page lists questions we have about your paper. The numbers displayed at left can be found in the text of the paper for reference. In addition, please review your paper as a whole for correctness.

"There are no Editor Queries for this paper"

TABLE OF CONTENTS LISTING

The table of contents for the journal will list your paper exactly as it appears below:

Buoyancy-Driven Continuous SPLITT Fractionation: A New Technique for Separation of Microspheres
Jonathan Storey, Phil Douglas, Phil Ligrani, and Karl Morten

3b2 Version Number : 7.51c/W (Jun 11 2001)
File path : P:/Santype/Journals/TandF_Production/LSST/v44n9/lsst395737/lsst395737.3d
Date and Time : 04/05/09 and 20:08

Separation Science and Technology, 44: 1–28, 2009

ISSN: 0149-6395 print/1520-5754 online
DOI: 10.1080/01496390902955651

Taylor & Francis
Taylor & Francis Group

Buoyancy-Driven Continuous SPLITT Fractionation: A New Technique for Separation of Microspheres

Jonathan Storey,[1] Phil Douglas,[1] Phil Ligrani,[1] and Karl Morten[2]
[1]Microfluidics Research Laboratory, Thermo-Fluids Laboratory, Department of Engineering Science, Parks Road, University of Oxford, Oxford, United Kingdom
[2]Nuffield Dept of Obstetrics and Gynaecology, University of Oxford, The Womens Centre John Radcliffe Hospital, Headington, Oxford, United Kingdom

Abstract: A new method of Continuous Fractionation using a SPLITT cell is conceived, developed, and tested, and is demonstrated to be useful for separation of collections of particles with different sizes and densities. With this previously uninvestigated mode of operation, this is accomplished for particles by *buoyancy-driven* separation. Some of the capabilities of this system are illustrated by successful separations of different-sized fluorescent polymer microspheres, with different carrier densities. The resulting experimentally-measured fraction recovery variations are then in good agreement with theoretical calculation from buoyancy-driven SPLITT theory.

Keywords: Buoyancy-driven fractionation, continuous SPLITT fractionation, separation of microspheres

Received 28 November 2008; accepted 9 March 2009.

Address correspondence to Phil Ligrani, Microfluidics Research Laboratory, Thermo-Fluids Laboratory, Department of Engineering Science, Parks Road, University of Oxford, Oxford, United Kingdom. E-mail: p_ligrani@msa.com

TRIBUTE TO DISTINGUISHED PROFESSOR CALVIN GIDDINGS.

The third author (PL) acknowledges an intellectual debt to Distinguished Professor Calvin Giddings for introducing him to SPLITT Fractionation and Field Flow Fractionation. This occurred as PL had the privilege of working with Professor Giddings for several years at the University of Utah, prior to his untimely death on October 24, 1996.

INTRODUCTION

SPLITT separation technology (here SPLITT is an acronym for Split-Flow Lateral-Transport Thin) makes use of thin (typically $<500\,\mu m$) and relatively broad channels (around 3 cm) to accomplish separations of particles based on their mobility in a transverse field in a short time. Channel lengths are also short and are generally of the order of 20 cm. This technology offers a number of advantages over competing technologies, such as continuous operation, good resolution, rapid sample separation and correspondingly high throughput (1). This technique has successfully been used with a number of different fields and experimental setups to accomplish the separation of a variety of particles from glass and polymer standards (2,3), to geological materials (4), to biological materials (5,6).

The theory is well-established and robust. SPLITT techniques are used with a variety of experimental setups, particle sizes and materials, and driving forces (2,6–9). Although using buoyancy forces as the principal driving force within a SPLITT cell has been proposed previously (7), and numerous papers describe buoyancy influences and effects on separations undertaken using different types of SPLITT cells (1,2), development of a buoyancy-driven cell has not, to the best of the authors' knowledge, been investigated until now.

Operating a SPLITT cell in buoyancy mode necessitates new methods of cell operation, and modified theoretical techniques to model the separations. The major difference, compared to sedimentation-based gravity-driven separation, is that the particles are less dense than the carrier fluid. In a gravitational SPLITT cell, the particles are introduced through an inlet at the top, and sediment from the top of the cell to the bottom of the cell. In a buoyancy-driven separation, the particles are introduced from the bottom of the cell, and migrate or float towards the top of the cell. The cell itself, however, can be identical to ones used in conventional gravitational SPLITT systems.

Separation of particles using either sedimentation-driven or buoyancy-driven SPLITT systems is possible when the particles have different sedimentation velocities. In conventional gravitational SPLITT systems, sedimentation velocities increase as particle size and particle density increase. In contrast, sedimentation velocities grow larger as particle size increases and particle density decreases in buoyancy driven SPLITT systems. Separations of small dense particles from larger, less-dense particles are therefore easier using buoyancy-driven separations, compared to gravitational–driven separations, because differences in sedimentation velocities of such particles are greater with buoyancy-driven separation. Using buoyancy as the driving force also allows

separation of the large particles from a mixture of other large particles, smaller particles of the same density, and denser impurities, all in one step, compared to the two that are generally required with a conventional gravitational SPLITT system. Buoyancy-based separation is especially useful in cases where the particles to be separated are less dense than the desired carrier fluid, particularly when cells or other biological particles are suspended in a denser biological buffer. In this situation, conventional gravitational SPLITT separation requires a different, less-dense carrier fluid, and the carrier fluid of choice may not be suitable. In contrast, the dense biological buffer is ideally suited for a buoyancy-driven separation of the associated cells and other biological particles. Our new buoyancy-driven SPLITT technique is thus especially applicable to cells, bacteria, pollen, hollow particles, low-density plastics and other similar particles, as well as a broad variety of other particles.

In the present paper, this new method of continuous fractionation using a Split-Flow-Lateral-Transport-Thin (SPLITT) cell is conceived, developed, and tested, and is demonstrated to be useful for the separation of collections of particles with different physical characteristics. This previously uninvestigated mode of operation relies on buoyancy-driven separation, and as such, uses buoyancy forces to separate particles based on their size and density. Some of the capabilities of this system are demonstrated as the buoyancy-driven SPLITT cell is used to separate 2.0 μm and 9.9 μm fluorescent polystyrene microspheres. These results illustrate the excellent performance of the cell, which is also verified by good agreement between experimental data and theoretical calculations from newly developed buoyancy-driven SPLITT theory. Experimental and theoretical results are also presented as the cell is operated with different carrier densities. The performance of the cell is qualified, and the operational and experimental procedures verified, using conventional gravitational-sedimentation modes of operation.

BACKGROUND AND THEORY

A schematic diagram of a SPLITT fractionation cell is shown in Fig. 1. This device has two inlets (a′ and b′) and two outlets (a and b). Fluid is pumped into the inlets, and a number of flow laminae are established. After particles are introduced into one of the inlets, they are displaced between laminae by a force acting in a direction perpendicular to the direction of flow. Differing flow rates lead to the creation of an inlet splitting plane (ISP), an outlet splitting plane (OSP) and a transport region between these two splitting planes. Particles which have sufficient

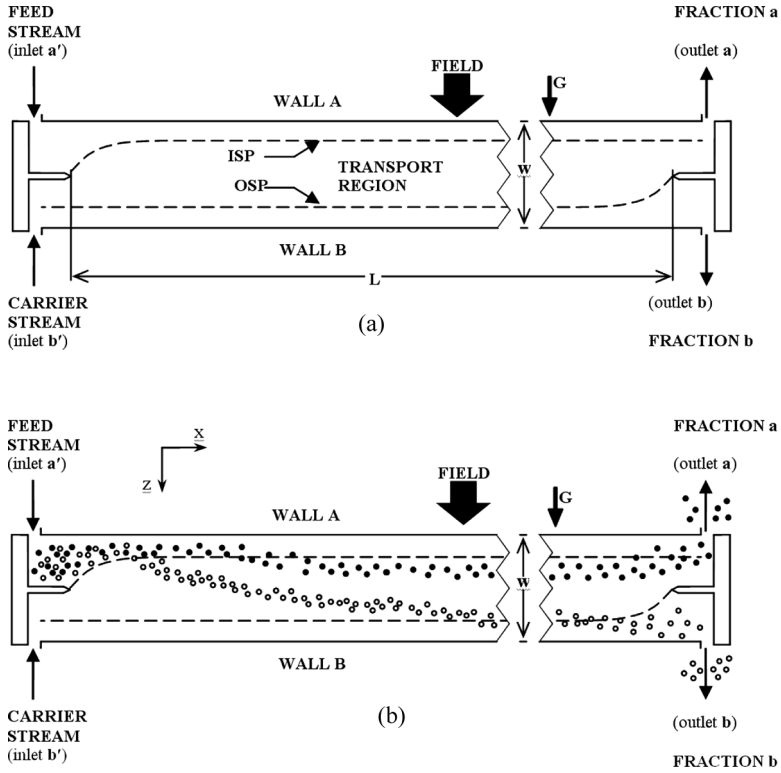

Figure 1. Schematic view of a SPLITT cell operating in sedimentation transport mode, showing (a) the overall layout of the cell, and (b) example particle trajectories during operation.

mobility to cross this transport region are directed to one outlet, whereas those with lower mobilities are advected to the other.

Principle – Sedimentation Mode

With the gravimetric SPLITT system, shown in Figs. 1(a) and 1(b), the particle sample is introduced through inlet a′ (8,9). Afterwards, the feed stream and the inlet splitting plane are displaced towards the top wall of the cell, as a result of unequal inlet flow rates, $\dot{V}(b') > \dot{V}(a')$. A gravitational field, acting across the cell, exerts a force upon the particles, causing those which are denser than the carrier fluid to sediment towards the bottom of the cell. The sedimentation velocity of the particles depends on the size of the particle, the difference in density between the fluid and the

particle, and the viscosity of the carrier. Particles with a sufficiently high sedimentation velocity cross the transport region, and are directed towards outlet b. Particles with lower sedimentation velocities are advected towards outlet a. For gravitational systems, the forces acting on such a particle include the weight of the particle, the buoyancy force acting on the particle, and the frictional force caused by the particle moving through a viscous fluid. When the weight of the particles is greater than the buoyancy force, the particle sinks, and when the buoyancy force is dominant, the particle floats. Note that the coordinate system for the gravimetric SPLITT system is included in Fig. 1(b).

Theory – Sedimentation Mode

The theory for sedimentation SPLITT fractionation considers the sedimentation velocity, U, which is the speed at which the particles descend through the carrier solution (10,11). This velocity is determined by assuming that the particle is spherical, the flow around the particle is laminar and Stokes' Law applies, and that the terminal velocity of the particles is reached quickly. For a spherical particle, the volume, V, is related to the diameter, d, using $V = (\pi/6)d^3$. The buoyant weight of a particle is then the difference between the weight of the particle and the buoyancy force acting on this particle. For a homogeneous particle of volume V, the weight is given by $\rho_p Vg$, while the buoyancy force acting on the particle is equal to the weight of the liquid the particle displaces, $\rho_c Vg$, ρ_c and ρ_p are the densities of the carrier fluid and the particle, respectively, and g is the acceleration due to gravity. The overall gravitational force, F_g acting on the a particle is therefore given by the buoyant weight of the particle

$$F_g = \rho_p Vg - \rho_c Vg = V(\rho_p - \rho_c)g = (\pi/6)d^3\Delta\rho g \tag{1}$$

where $\Delta\rho = (\rho_p - \rho_c)$. The frictional force acting on a spherical particle from Stokes' Law is given as

$$F_d = 6\pi\eta uR = 3\pi\eta ud \tag{2}$$

where u is the velocity of particle motion. At terminal velocity, U, the gravitational force and the frictional force are equal, $F_g = F_d$, which means that

$$(\pi/6)d^3\Delta\rho g = 3\pi\eta dU \tag{3}$$

The sedimentation velocity, U, is then given by

$$U = \frac{(\pi/6)d^3\Delta\rho g}{3\pi\eta d} = \frac{\Delta\rho g d^2}{18\eta} \tag{4}$$

The volumetric flow rate, $\dot{V}(t)$, of the transport region is defined as the difference between the flow rates at the inlet a′ where the particles are introduced, and outlet a

$$\dot{V}(t) = \dot{V}(a) - \dot{V}(a') = \dot{V}(b') - \dot{V}(b) \tag{5}$$

In order for a particle introduced at inlet a′ to exit the diagonally opposite outlet (in this case, outlet b), the particle must sediment through the transport region. The volumetric flow rate of the lamina across which a particle sediments, $\Delta\dot{V}$, is given by

$$\Delta\dot{V} = bLU = \frac{bL(\rho_p - \rho_c)gd^2}{18\eta} \tag{6}$$

This equation is based upon particle advection in the positive x direction by the flow at a streamwise velocity v, and sedimentation in the z direction with sedimentation velocity U. Over time dt the particle migrates a distance $dz = Udt$ in the z direction, and a distance $dx = vdt$ in the x direction. This gives the relationship $dx/v = dz/U$. The streamwise velocity of a lamina of thickness dz is equal to the incremental volumetric flow rate in that lamina, divided by the cross section of the lamina $v = d\dot{V}/bdz$. Combining these results gives $dx = d\dot{V}/bU$, which, after integration, becomes $\Delta\dot{V} = bUL$ noting that the integral of dx over the length of the channel is L, the channel length. According to Giddings (8,10), Springston et al. (9), and Gupta et al. (11), particles introduced close to the inlet splitting plane (ISP) are recovered at outlet a provided

$$\Delta\dot{V} \leq \dot{V}(t) \tag{7}$$

Particles are recovered at outlet b if

$$\Delta\dot{V} > \dot{V}(t) \tag{8}$$

The fraction of particles recovered at outlet b (F_b) and the corresponding recovery at outlet a (F_a) are subsequently given by

$$F_b = \frac{\Delta\dot{V} - \dot{V}(t)}{\dot{V}(a')} = \frac{\Delta\dot{V} - \dot{V}(a)}{\dot{V}(a')} + 1 \tag{9}$$

and

$$F_a = 1 - F_b \tag{10}$$

respectively. Note that Eq. 9, when combined with Eq. 6, shows linear dependence of recovery factor F_b on carrier density ρ_c. The total flow rate through the cell $\dot{V}_{tot}$ is equal to the sum of the flow rates at the inlets, and also to the sum of the flow rates at the outlets

$$\dot{V}_{tot} = \dot{V}(a') + \dot{V}(b') = \dot{V}(a) + \dot{V}(b) \tag{11}$$

If diagonally opposite flow rates are set equal, then

$$\dot{V}(a') = \dot{V}(b) \tag{12}$$

and

$$\dot{V}(b') = \dot{V}(a) \tag{13}$$

Eqs. 5, 11 and 13 can then be combined and rearranged, to give

$$\dot{V}_{tot} = \dot{V}(a') + \dot{V}(b') = \dot{V}(a') + \dot{V}(a) \tag{14}$$

$$\dot{V}_{tot} = [\dot{V}(a) - \dot{V}(a')] + \dot{V}(a') + \dot{V}(a') \tag{15}$$

and

$$\dot{V}_{tot} = \dot{V}(t) + 2\dot{V}(a') \tag{16}$$

Eqs. 9 and 16 may be combined to give F_b, the fractional recovery at outlet b, as it depends upon the total flow rate $\dot{V}_{tot}$ and the flow rate at inlet a′ $\dot{V}(a')$. The resulting equation is given by

$$F_b = \frac{\Delta\dot{V} - \dot{V}(t)}{\dot{V}(a')} = \frac{\Delta\dot{V} - \dot{V}_{tot}}{\dot{V}(a')} + 2 \tag{17}$$

The flow rate at inlet a′ that is required to obtain a desired F_b is then obtained using

$$\dot{V}(a') = \frac{\Delta\dot{V} - \dot{V}_{tot}}{[F_b - 2]} \tag{18}$$

where $\Delta\dot{V}$ is determined using Eq. 6, and $\dot{V}_{tot}$ is determined using Eq. 11. As such, Eqs. 12–18 are valid when diagonally-opposite flow rates are

equal. Such results are then useful to illustrate the flow rate conditions required to achieve levels of separation, quantified by the magnitudes of F_a and F_b.

Principle – Buoyancy Mode

Buoyancy driven SPLITT fractionation is illustrated schematically in Figs. 2(a) and 2(b). With this arrangement, the particles in the sample are generally less dense than the carrier fluid. The particles are therefore buoyant, and float. The resulting buoyancy force is caused by hydrostatic pressure acting on a particle and is equal to the weight of fluid displaced by a particle. Acting in the opposite direction is the gravitational force acting on a particle, which equals the weight of the particle. When particles are less dense than the carrier, the weight of the displaced carrier fluid (and hence the buoyancy force acting on the particle) is greater than the weight of the particle. The net force acting on the particle is therefore upwards and so the particle floats as it moves towards the upper wall of the SPLITT Fractionation cell. Particles are introduced through inlet b′, where ones with high mobility, the greatest buoyancy forces, and a sufficiently large flotation velocity, cross the transport region to exit the cell at outlet a. Particles with lower transport velocities then exit through outlet b. Of course, this arrangement is opposite to the situation found in conventional gravitational SPLITT systems.

Theory – Buoyant Mode

The sedimentation velocity, U, here, referred to as the flotation velocity, is again given by Eq. 4 except that U and $\Delta\rho$ are now negative. This means that particles move upwards through the cell, in the negative z direction. The volumetric flow rate of the transport region, $\dot{V}(t)$, considers that the particle inlet is now b′ to give

$$\dot{V}(t) = \dot{V}(b) - \dot{V}(b') \tag{19}$$

For a particle introduced at inlet b′ to exit the diagonally opposite outlet (now outlet a), the particle must float through the transport region towards the upper wall of the cell. Consider a particle still carried in the positive x direction by the flow at a velocity v, but now moving the $-z$ direction with velocity U. The resulting relationship between velocity and displacement is given as $dx/v = -dz/U$. After rearrangement, this relationship becomes

$$dx = -d\dot{V}/bU \tag{20}$$

which, after integration, yields

$$\Delta\dot{V} = -bUL \tag{21}$$

noting once again that the integral of dx over the length of the channel yields L, the channel length. Since particles must now move in the $-z$ direction to be directed to the opposite outlet, combining Eqs. 4 and 21 yields the volumetric flow rate of the lamina crossed by the particle, which is subsequently given by

$$\Delta\dot{V} = -bLU = -\frac{bL(\rho_p - \rho_c)gd^2}{18\eta} \tag{22}$$

If one considers that particles are introduced through inlet b′, and that sufficient sedimentation leads to particle recovery at outlet a, then, fractional recovery at outlet a, for the buoyancy induced arrangement shown in Figs. 2(a) and 2(b) is expressed using

$$F_a = \frac{\Delta\dot{V} - \dot{V}(t)}{\dot{V}(b')} = \frac{\Delta\dot{V} - \dot{V}(b)}{\dot{V}(b')} + 1 \tag{23}$$

The fractional recovery at outlet b, is then given by

$$F_b = 1 - F_a \tag{24}$$

From Eqs. 22 and 23, it is evident that recovery fraction F_a shows linear dependence upon carrier density ρ_c. If diagonally opposite flow rates are again set equal, Eqs. 11, 12, and 19 can subsequently be combined to produce

$$\dot{V}(a') = \dot{V}(b) \tag{25}$$

$$\dot{V}(b') = \dot{V}(a) \tag{26}$$

$$\dot{V}_{tot} = \dot{V}(a') + \dot{V}(b') = \dot{V}(b) + \dot{V}(b') \tag{27}$$

and

$$\dot{V}_{tot} = \dot{V}(t) + 2\dot{V}(b') \tag{28}$$

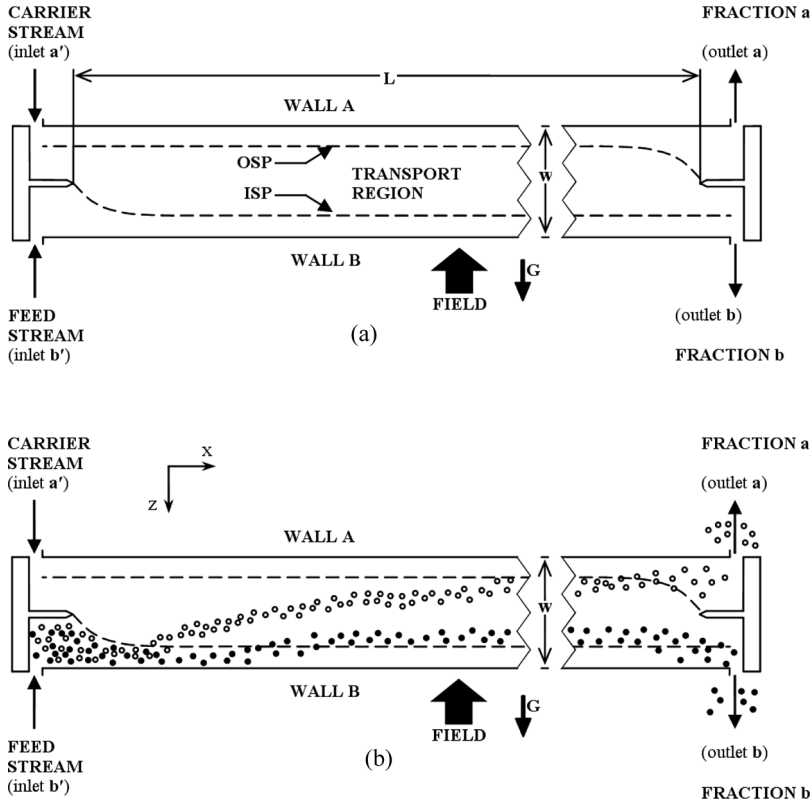

Figure 2. Schematic view of a SPLITT cell operating in buoyancy-driven transport mode, showing (a) the overall layout of the cell, and (b) example particle trajectories during operation.

Further rearrangement of Eqs. 23 and 28 subsequently yields

$$F_a = \frac{\Delta\dot{V} - \dot{V}(t)}{\dot{V}(b')} = \frac{\Delta\dot{V} - \dot{V}_{tot}}{\dot{V}(b')} + 2 \tag{29}$$

The flow rate at inlet b′, given as $\dot{V}(b')$, is then expressed using

$$\dot{V}(b') = \frac{\Delta\dot{V} - \dot{V}_{tot}}{[F_a - 2]} \tag{30}$$

This equation then allows determination of the flow rate $\dot{V}(b')$ which is required to produce fractional recovery F_a with buoyancy-induced SPLITT fractionation, provided diagonally-opposite flow rates are equal.

EXPERIMENTAL APPARATUS, MATERIALS, AND CONDITIONS

SPLITT Fractionation Channel

The results presented in this paper are obtained using a SPLITT channel fabricated in the main workshop for the Thermo-Fluids Laboratory, from stock materials. Figure 3 shows a picture of the channel used; it is a typical SPLITT channel (8–11), comprising glass walls, mylar spacers and a stainless steel splitter. Figure 4 shows how these parts are assembled.

The plates that make up the walls of the cell are made of float glass coated with Pluronic F127 Prill (BASF, Cat # 30087870). Float glass is used for the walls as it is smooth and, as such, minimizes flow disturbances. The glass is also inert and mechanically stable. It also enables direct observation of cell conditions, for example to check for the presence of bubbles that, if present, disturb the flow. Pluronic-coating of the glass increases the hydrophilicity of the surface, and so helps prevent bubbles becoming lodged in the cell. Mylar is used for the spacers due to its mechanical and chemical stability, and the ready availability of the thickness required. The splitter is made from steel in order to provide a rigid device without any flexing and distortion which could create flow disturbances.

The channel design is simple, with tapered inlets and outlet to distribute the flow over the breadth of the channel. The stainless steel splitter is 225 μm thick, while the mylar spacers are each 130 μm thick. This gives a total channel thickness of 485 μm. The entire system is clamped using 2 Perspex blocks; the bolts are tightened to 2 Nm using a torque wrench.

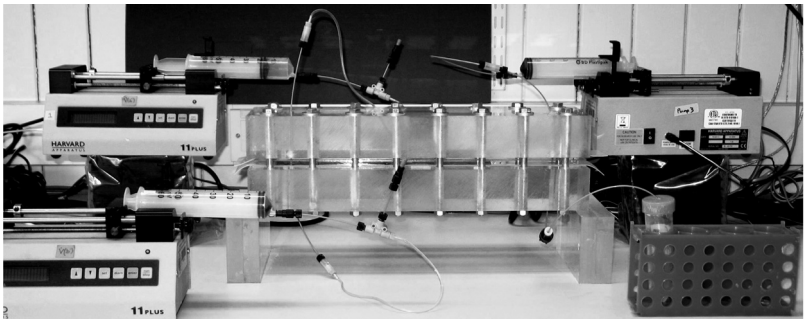

Figure 3. Photograph of the cell for the sedimentation-driven and buoyancy-driven experiments.

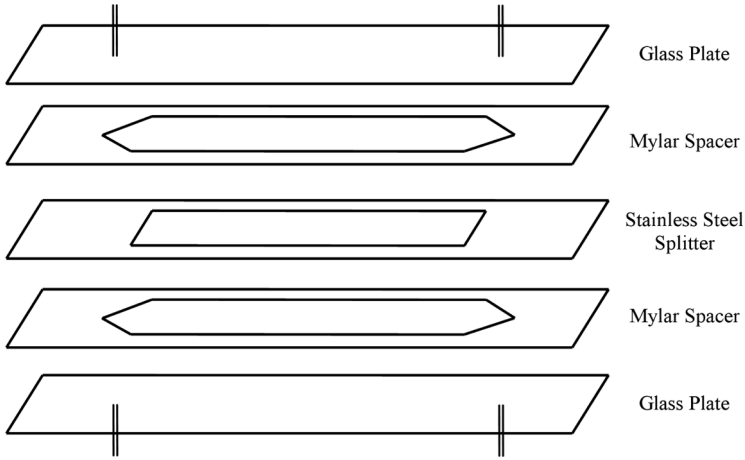

Figure 4. Schematic diagram showing an overview of the cell construction and layout.

This is sufficient to prevent leaks in the cell. The overall length of the splitting region is 20 cm, its breadth 3 cm and width 485 μm. The dimensions chosen for our channel mean that separation of the particles used can be achieved with moderate to low flow rates, and over reasonable times.

Pumps and Fittings

The overall schematic of the experimental setup is shown in Fig. 5. Pumps are used to set the flow rates at two of the inlets and one outlet, which in turn fixes the flow rate at the other outlet. The pumps are

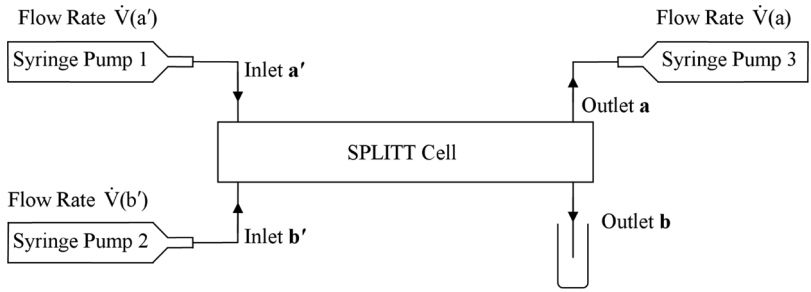

Figure 5. Schematic diagram showing flow connections to and from the cell, and the arrangement of the syringe pumps.

Harvard Apparatus 11-Plus syringe pumps (model numbers 70-2211 or 70-2208) fitted with 50 mL BD Plastipak Syringes (Cat # 300866). These syringe pumps allow accurate, rapid, and reliable setting of flow rates and provide a smooth, pulse-free flow of liquid at the flow rates used in this study. Syringe pumps are used in preference to peristaltic pumps, since peristaltic pumps occasionally cause unacceptable pulsing of the fluid in the cell. Such pulsing can lead to mixing of the laminae, reducing the resolution of the system. Connections are made with 0.75 mm ID PEEK Tubing (Upchurch Scientific, Cat # 1533 L). A tee (Upchurch Scientific, Cat # P-714-01) followed by 10 cm of Tygon LFL Tubing (0.89 mm ID, Cat # 96429-26) is added in-line to each of the inlets, to enable the system to be primed more easily and the inlet flows to be checked for bubbles. When the tees are not being used for priming, they are sealed with rubber bungs.

Instrumentation

The samples that are collected at each outlet are analysed to determine the number of each type of bead in the sample. This can then be used to calculate the fraction of each particle size exiting each outlet. This is accomplished by first measuring the mass of each sample collected, using an Acculab Atilon ATL-124 balance. This mass is then related to the total volume of sample collected, by knowledge of the carrier density. Using a micropipette (Gilson Pipetman P200), 200 μL per well of each sample is added to a 96 well plate (BD Falcon Microtest Plate, Ref: 353293) in triplicate, and the average fluorescent intensity determined by use of a Tecan Infinite F200 Plate Reader with Magellan 6 Software.

The average fluorescence, $\overline{F}$, of the wells is directly proportional to the average number of beads per well ($\overline{F} \propto \bar{n}_{well}$), which, in turn, is directly proportional to the bead concentration in the sample ($\bar{n}_{well} \propto [Beads]$) since a constant volume is added to each well. A measure of the relative number of beads in each sample can then be obtained by multiplying the average fluorescent intensity recorded for the well by the sample volume ($n_{sample} \propto [Beads] \times V_{sample}$; $[Beads] \propto \bar{F}$). From this, the fraction of beads exiting outlet a is determined using $F_a = n_a/(n_a + n_b)$, and the fraction exiting outlet b is subsequently found using $F_b = n_b/(n_a + n_b)$.

Fluorescent Beads

The different sized particles used in this study are fluorescent, monodisperse particle standards, which offer excellent experimental repeatability

and good confidence in particle size. In addition, the fluorescence means that accurate determination of the concentration of the beads in the samples collected is both simple and robust.

9.9 μm and 2.0 μm fluorescent polymer microspheres are supplied as aqueous suspensions by Duke Scientific (distributed by Brookhaven Instruments Ltd., Worcestershire, UK). Catalogue numbers of the beads used are G1000 (9.9 μm green fluorescent beads) and R0200 (2.0 μm red fluorescent beads). To prevent differences between lots causing discrepancies, all data presented are from the same lot number of each set of beads. Using fluorescent beads of different colors allows the number of beads of one size to be rapidly and accurately determined, even in the presence of beads of the other size. This makes it far easier to analyse the mixtures of beads produced in the experiments. 2 differing values of the bead density can be found in literature provided by Duke Scientific (1.05 g cm^{-3} and 1.06 g cm^{-3}). The average of these values (1055 kg m^{-3}) is the value used to calculate quantities related to the theoretical analyses.

Carrier Fluid

Preparation of the sample is the same for both sedimentation and buoyancy experiments. The sample stock for a given experiment is prepared by diluting the original bead suspension 1 in 100 (v/v) with the carrier stock that is to be used in that experiment. The samples are degassed using a vacuum prior to using them in an experiment.

The standard carrier solution in use in these experiments is MilliQ Water with 0.05% (v/v) Tween 20 (Sigma, Cat # P1379). Degassing using a vacuum is performed prior to using the solution in an experiment. Tween 20 is added to the solution to help prevent bubbles sticking in the cell, by increasing the affinity of the carrier for the walls. Without it, the bubbles have a tendency to remain lodged in the SPLITT cell.

To prepare the solutions of varying density for the variable density and buoyancy sets of experiments, sodium chloride (Sigma, Cat # S9625) is added to the 0.05% Tween 20 solution. Sodium chloride is used because it is relatively harmless, it does not cause excessive damage to the materials used within the cell, and it can easily be dissolved in water to produce solutions of the densities required. Carrier fluids with different densities are prepared by making up two stock solutions:

1. 0.05% Tween 20 solution, and
2. 0.05% Tween 20 + 18% (weight by volume) NaCl.

Once the density of these solutions are determined, solutions of intermediate density are prepared by mixing varying proportions of these two solutions. Prior to using these solutions in the variable density experiments, their density is measured using the procedures described below. For the buoyancy experiments, the percentage (weight by volume) of NaCl required to produce a solution of the desired density is calculated based on data from the CRC Handbook (12). Solutions prepared to include this percentage of NaCl are made, and the density of each solution prepared is again measured prior to use. The densities of the solutions are determined by weighing 6 replicates of a known volume of solution, and then, by taking the average density from these 6 replicates. The viscosity of the solution is then determined from data for aqueous sodium chloride solutions which relate density and viscosity from the CRC Handbook (12).

Priming the SPLITT Fractionation Cell

The presence of bubbles in the cell severely disturbs the flow of fluid through the system, because they divert the flow of the liquid around them, and subsequently cause mixing of the flow laminae, which severely degrades system resolution. These bubbles occasionally remain trapped within the cell, despite the use of Tween 20 in the carrier solution. Care is thus taken to minimize the presence of bubbles. This is accomplished prior to each experiment by priming the system by first flushing the system with carrier fluid from inlets a′ and b′, at a rate of 5 mL/min. While this is ongoing, pure methanol from Rathburn Chemicals Ltd (Cat # RH1019) is injected using the T junctions connected to inlets a′ and b′. This causes the bubbles to move through the system towards the outlets. Finally, bubbles which remain directly adjacent to the outlet splitter are removed by again injecting pure methanol into outlet a, forcing the bubbles out through outlet b. When this has been done, sufficient carrier fluid is pumped through the cell to ensure that all of the methanol is purged from the system. The system is subsequently checked for the presence of bubbles prior to each experiment. If any are present, the system is then primed again.

Flow Establishment within the SPLITT Fractionation Cell

Prior to the start of sample collection, flow through the cell is established to minimize the detrimental effects of transient phenomena on system performance. During flow establishment, both of the cell outlets are

disconnected and left open, while the carrier fluid and the sample are pumped in the relevant inlets at the same flow rate which is used during sample collection. When the flow establishment is completed, outlet a is connected to the syringe pump, and sample collection is started without interrupting the flows at the two inlets. This procedure is followed because of the flow disturbances which occur when flow through the cell is initiated. Even though such start-up disturbances rapidly diminish, they can cause mixing between fluid streams. With the present arrangement, steady flow is established without such transient disturbances prior to the collection of samples. Transient disturbances thus do not affect the fractional recovery of the particles. This is accomplished because the present data are for experiments lasting either 20 minutes, with 5 minutes of flow establishment time followed by 15 minutes of sample collection time, or 40 minutes, with 10 minutes of flow establishment time followed by 30 minutes of sample collection time.

EXPERIMENTAL RESULTS

Data are presented here from four sets of experiments. The first set comprises experiments with the cell operating in sedimentation mode. The second set comprise experiments performed using both the sedimentation and buoyancy modes. Here, the carrier density is varied in order to change the fraction of beads exiting a given outlet. The third and fourth sets of experiments comprise separations of beads using the new buoyancy mode of operation with two different magnitudes of carrier density.

Channel Characterization in Sedimentation Mode

This set of experiments is employed to confirm that the channel operates, as expected, with normal performance and standard operating conditions, in the sedimentation mode. The results from three sets of individual experiments, performed with polymer microspheres of differing sizes, are presented. These experiments show that the measured recovery fractions agree with theory at a variety of flow rates, and that mixtures of beads are separable using the system. Data from the first set, using only 2.0 μm beads, are presented in Fig. 6. Results from the second set of experiments, using only 9.9 μm beads, are presented in Fig. 7. The data presented in Fig. 8 are from third set of experiments, and shows the results from experiments which use a mixture of 2 μm and 9.9 μm beads. The sample solution is introduced through inlet a′ within these experiments, as shown in Figs. 1(a) and 1(b). Beads which are denser than the carrier fluid are

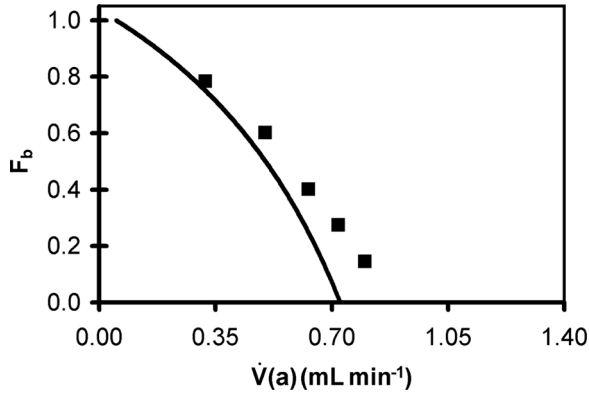

Figure 6. Variation of the fractional recovery at outlet b (F_b) with flow rate $\dot{V}(a)$ of 2 μm polystyrene microspheres in sedimentation mode. The total flow rate ($\dot{V}_{tot}$) through the cell is 1.4 mL min^{-1}. Symbols are defined in Fig. 8.

used. Those beads with greater sedimentation velocities move towards outlet b, while beads with lower sedimentation velocities are carried to outlet a.

The total flow rate $\dot{V}_{tot}$ through the cell is 1.4 mL min^{-1} for all of these experiments. In addition, flows diagonally opposite each other are equal so that Eqs. 12 and 13 are satisfied, along with Eq. 11. With this arrangement, knowledge of any one flow rate then allows all of the other flow rates to be determined. Flow rates used in the data presented

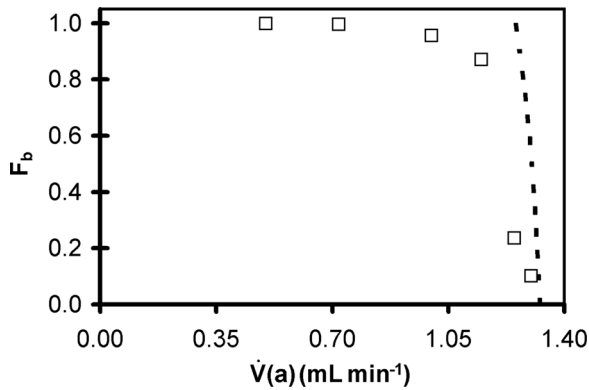

Figure 7. Variation of the fractional recovery at outlet b (F_b) with flow rate $\dot{V}(a)$ of 9.9 μm polystyrene microspheres in sedimentation mode. The total flow rate ($\dot{V}_{tot}$) through the cell is 1.4 mL min^{-1}. Symbols are defined in Fig. 8.

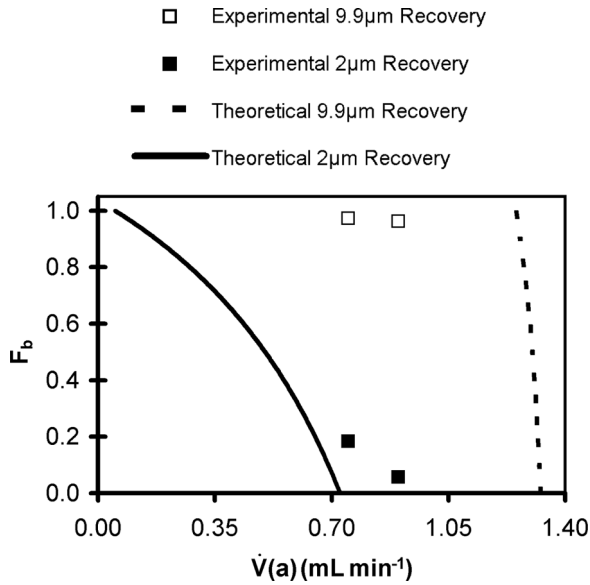

Figure 8. Variation of the fractional recovery at outlet b (F_b) with flow rate $\dot{V}(a)$ of a mixture of 2 μm and 9.9 μm polystyrene microspheres in sedimentation mode. The total flow rate ($\dot{V}_{tot}$) through the cell is 1.4 mL min^{-1}.

vary from $\dot{V}(a') = 0.10$ mL min^{-1} and $\dot{V}(b') = 1.30$ mL min^{-1} to $\dot{V}(a') =$ 1.08 mL min^{-1} and $\dot{V}(b') = 0.32$ mL min^{-1}. Thus, as the total channel flow rate is kept constant at 1.4 mL min^{-1}, $\dot{V}(a')$ varies from 0.10 mL min^{-1} to 1.08 mL min^{-1}. Results are presented for experiments which last for 20 minutes, with 5 minutes of flow establishment time and 15 minutes of sample collection time. The only exception is with two 9.9 μm particle experiments with $\dot{V}(a') = 0.40$ mL min^{-1}, where sample collection time is 20 minutes, and for $\dot{V}(a') = 0.15$ mL min^{-1} and 0.10 mL min^{-1}, where sample collection time is 30 minutes. Increased sample collection times mean that flow establishment times are also increased accordingly.

Figure 6 shows that, as the flow rate at outlet a $\dot{V}(a)$ increases, the fraction of 2.0 μm polystyrene microsphere beads recovered from outlet b, F_b, decreases. Thus, the direction of the 2.0 μm beads to different outlets is altered as $\dot{V}(a)$ is changed. The explanation for this general trend is that, as $\dot{V}(a)$ increases, $\dot{V}(a')$ decreases correspondingly since the total flow rate, $\dot{V}_{tot}$, is fixed by Eq. 11. The volumetric flow rate of the transport region, $\dot{V}(t)$, therefore increases according to Eq. 5. This leads to a decrease in the fraction of particles exiting outlet b, according to Eq. 9.

Figure 6 also shows good agreement between measured and theoretical values of F_b as this quantity varies with $\dot{V}(a)$. Note that theoretical F_b values equal 0.0 for $\dot{V}(a) > 0.73$ and equal 1.0 for $\dot{V}(a) < 0.05$. Theoretical lines are determined using properties of pure water for the carrier density and viscosity, as determined from the CRC Handbook (12). The carrier density used for the calculations is 997.048 kg m^{-3}; the carrier viscosity used is 0.000890 Pa s.

Figure 7 shows that, as the flow rate at outlet a $\dot{V}(a)$ increases, the fraction of 9.9 μm polystyrene microsphere beads recovered from outlet b, F_b, decreases. Thus, the direction of 9.9 μm beads to different outlets is altered as $\dot{V}(a)$ is changed. The reasons for this trend are the same as for the 2 μm beads. However, in this case, the larger particle size means that the $\dot{V}(a)$ flow rate is higher than for the 2 μm beads to achieve the same magnitudes of F_b fraction recovery. The volumetric flow rate of the lamina crossed by a particle $\Delta\dot{V}$ depends on the square of the particle diameter according to Eq. 6. Since the 9.9 μm particles have a greater diameter, the volumetric flow rate of the lamina crossed by the particle is much greater. Thus, according to Eq. 9, for the same volumetric flow rate of the transport region $\dot{V}(t)$, the fraction of particles recovered at outlet b, F_b, is lower. Such trends are confirmed by good agreement between experimental data and theoretical predictions in Figs. 6 and 7. In Fig. 7, theoretical F_b values equal 1.0 for $\dot{V}(a)$ magnitudes less than 1.20.

The results presented in Fig. 8 are for experiments undertaken to confirm that separation of a mixture of different sized beads is successfully achieved with the present channel. This figure shows that the majority of 9.9 μm beads are directed to outlet b since the fraction of the 9.9 μm collected at outlet b, F_b, is close to 1. The majority of 2 μm beads, on the other hand, are directed to outlet a. In other words, the fraction of the 2 μm beads collected at outlet b, F_b, is close to 0, which means that the fraction collected at outlet a, F_a is close to 1 according to Eq. 10. This is because $\Delta\dot{V} \leq \dot{V}(t)$, the volumetric flow rate of the lamina across which the 2 μm beads sediment $\Delta\dot{V}$ is smaller than the volumetric flow rate of the transport region, while $\Delta\dot{V} > \dot{V}(t)$ for the 9.9 μm beads. Efficient separation is achieved because the majority of 9.9 μm beads is directed towards one outlet, while the majority of the 2.0 μm beads is directed towards the other outlet.

Combining Eqns. 6, 9, and 11 gives the following equation for the dependence of F_b on $\dot{V}(a)$.

$$F_b = \frac{\left[\frac{bL(\rho_p - \rho_c)gd^2}{18\eta}\right] - \dot{V}(a)}{\dot{V}_{tot} - \dot{V}(a)} + 1 \tag{31}$$

From this equation, it is evident that recovery fraction F_b is dependent upon $\dot{V}(a)$ in a non-linear fashion. This is consistent with the experimental results in Figs. 6, 7, and 8, wherein the total flow rate $\dot{V}_{tot}$ is kept constant, which also show non-linear behavior, especially as F_b varies with $\dot{V}(a)$ for the 2.0 μm particles.

Our early work on sedimentation SPLITT systems shows that the resolution of the system is sometimes dramatically reduced when $\dot{V}(a)$, the flow rate through outlet a, is either many times larger or smaller than $\dot{V}(b)$, the flow rate through outlet b. When this occurs, the fraction of beads directed to an outlet appears to be proportional to the fraction of the total flow through that outlet, regardless of the size of the particles. This appears to occur as the large difference in flow rates causes the laminae to mix, thereby perturbing the laminar flow. This may then result in some local turbulence motions, which decreases the fractionation resolution of the gravimetric SPLITT system.

Sedimentation and Buoyancy Modes of Behavior with Varying Carrier Densities

This series of experiments shows how the fractionation system responds when the density of the carrier solution is adjusted. One set of data, presented in Fig. 9, shows results obtained with the cell operating in the sedimentation mode. The other set of data, presented in Fig. 10,

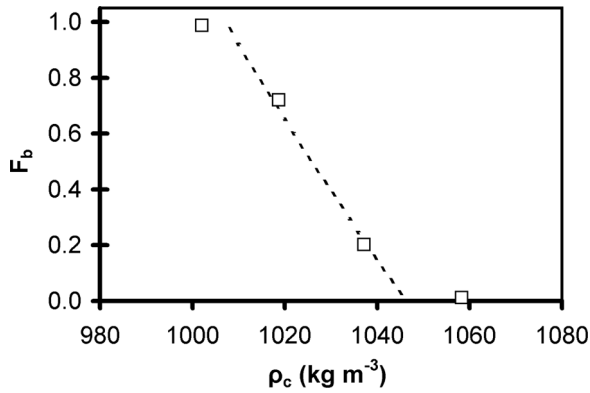

Figure 9. Variation of the fractional recovery at outlet b (F_b) with carrier density (ρ_c) of 9.9 μm polystyrene microspheres in sedimentation mode. The flow rates are: $\dot{V}(a') = 0.75\,\text{mL min}^{-1}$, $\dot{V}(b') = 0.90\,\text{mL min}^{-1}$, $\dot{V}(a) = 0.90\,\text{mL min}^{-1}$ and $\dot{V}(b) = 0.75\,\text{mL min}^{-1}$. Symbols are defined in Fig. 8.

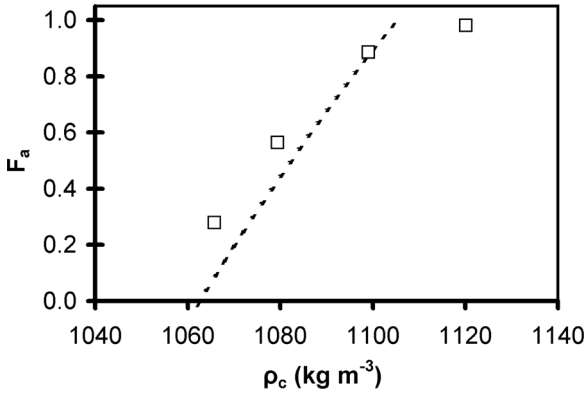

Figure 10. Variation of the fractional recovery at outlet a (F_a) with carrier density (ρ_c) of 9.9 μm polystyrene microspheres in buoyancy-driven mode. The flow rates are: $\dot{V}(a') = 0.725\,\text{mL min}^{-1}$, $\dot{V}(b') = 0.60\,\text{mL min}^{-1}$, $\dot{V}(a) = 0.60\,\text{mL min}^{-1}$ and $\dot{V}(b) = 0.725\,\text{mL min}^{-1}$. Symbols are defined in Fig. 8.

presents results obtained with the cell operating in the buoyancy-driven mode. In both cases, the carrier density is altered as the volumetric flow rate of the transport region $\dot{V}(t)$ is kept constant. This arrangement changes U, the sedimentation velocity or flotation velocity of the beads, as well as the volumetric flow rate of the lamina across which the sediment $\Delta\dot{V}$. When the cell operates in the sedimentation mode, the sample is introduced through inlet a′. When the cell operates in the buoyancy mode, the sample is introduced through inlet b′. With the sedimentation mode, flow rates $\dot{V}(a') = 0.75\,\text{mL min}^{-1}$, $\dot{V}(b') = 0.90\,\text{mL min}^{-1}$, $\dot{V}(a') = 0.90\,\text{mL min}^{-1}$, and $\dot{V}(b) = 0.75\,\text{mL min}^{-1}$ are employed. With the buoyancy mode, flow rates $\dot{V}(a') = 0.725\,\text{mL min}^{-1}$, $\dot{V}(b') = 0.60\,\text{mL min}^{-1}$, $\dot{V}(a) = 0.60\,\text{mL min}^{-1}$ and $\dot{V}(b) = 0.725\,\text{mL min}^{-1}$ are employed. In all cases, the experiment duration is 20 minutes, with 5 minutes of flow establishment time followed by 15 minutes of sample collection time. Carrier viscosity is determined from density data from the CRC Handbook (12) for a pure NaCl solution.

Figure 9 shows that increasing the density of the carrier solution results in a decrease in the fraction of beads exiting outlet b with the sedimentation mode of operation, wherein the particles are more dense than the carrier fluid. This is consistent with theoretical predictions which indicate that a smaller fraction of the particles exits outlet b as the difference in density between the carrier and the particles decreases. Equation 4 shows that this is because the sedimentation velocity decreases as the density difference between the carrier and the particles decreases, which corresponds with a decrease of the volumetric flow rate of the lamina

crossed by the particle according to Eq. 6. Equations 9 and 17 then confirms the decrease of fractional recovery at outlet b, as the carrier density increases.

With the buoyancy mode of operation, Fig. 10 shows that increasing the carrier density increases F_a, the fraction of beads exiting outlet a, since the buoyancy forces acting on the particles are greater. Such behaviour is consistent with Eqs. 22, and 23, which show that the fraction beads exiting outlet a increases as the difference in density between the beads and the carrier increases. This is because Eq. 4 shows that the flotation velocity becomes more negative as the density difference between the carrier and the particle increases, which means that the volumetric flow rate of the lamina crossed by the particle increases according to Eq. 22. Equation 23 then indicates that the fractional recovery at outlet a increases as the carrier density increases.

Figures 9 and 10 also show that the theoretical and experimental results match fairly closely. This provides confidence that the existing SPLITT fractionation theory for the sedimentation mode, as well as the theory for the buoyancy mode, can be applied to a wide range of experimental conditions with different carrier densities with confidence. Another interesting characteristic of the results in Figs. 9 and 10 is the approximately linear dependence of F_b on ρ_c in the first figure and F_a on ρ_c in the second figure, which is consistent with Eqs. 6, 9, 22, and 23.

Buoyancy-Driven Separation of Particles, Carrier Density of 1133.9 to 1138.8 Kg M^{-3}

Here, results from the third and fourth sets of experiments, mentioned earlier, are presented. Additional verification is provided that the buoyancy-induced mode of SPLITT fractionation provides excellent separation resolution and performance, which are in agreement with the theory for the buoyancy-driven mode. For the third set of experiments, data from two collections of experiments are presented in Fig. 11. Here, carrier densities are 1133.9 kg m^{-3} and 1138.8 kg m^{-3}.

With the buoyancy-driven SPLITT arrangement, the carrier density is greater than that of the particles. Larger particles then displace more carrier fluid, and thus experience a greater buoyancy force. This force causes the flotation velocity U of larger particles to be greater, which means that larger particles move more readily towards outlet a than smaller particles of the same density. This causes F_a, the fraction of the larger particles recovered at outlet a, to increase relative to the fraction of smaller particles recovered at outlet a. In all cases, the sample is introduced into the cell through inlet b′. The total sample flow rate $\dot{V}_{tot}$ is 0.7 mL min^{-1} and

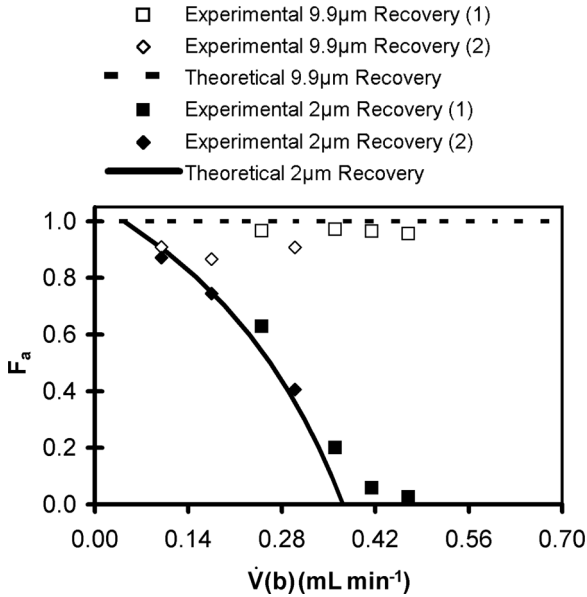

Figure 11. Variation of the fractional recovery at outlet a (F_a) with flow rate $\dot{V}(a)$ of a mixture of 2 μm and 9.9 μm polystyrene microspheres in buoyancy-driven mode. The total flow rate ($\dot{V}_{tot}$) through the cell is 0.7 mL min^{-1}. NaCl is added to adjust the carrier density. Data from two sets of experiments are presented. The first set of experiments (1) uses a carrier where $\rho_c = 1133.9$ kg m^{-3}. The second set of experiments (2) uses a carrier where $\rho_c = 1138.8$ kg m^{-3}.

flows diagonally opposite each other are equal in all cases. All other flow rates can therefore be determined from knowledge of one flow rate using Eqs. 25–27. The time for each experiment is 40 minutes, with 10 minutes of flow establishment time, followed by 30 minutes of sample collection time. Exceptions are the final two experiments of the fourth set of buoyancy experiments, where $\dot{V}(a') = 0.53$ mL min^{-1} and $\dot{V}(a') = 0.6$ mL min^{-1}, and where the experiment duration is 30 minutes, with 5 minutes of flow establishment time followed by 25 minutes of sample collection time.

Theoretically predicted fractional recovery values are determined using the measured carrier density and the calculated carrier viscosity. The viscosity is determined using data from the CRC Handbook (12) for a pure NaCl solution. For the first data collection set in the third set of experiments, the value of measured carrier density used in calculations is 1133.9 kg m^{-3} and viscosity is 0.001478 Pa s (Fig. 11, set (1)). For the second data collection set for the third set of experiments, the carrier

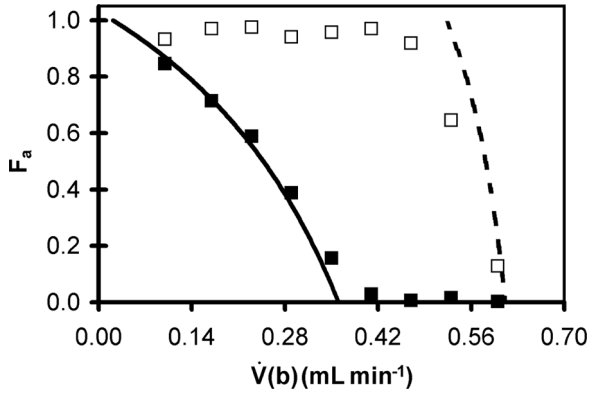

Figure 12. Variation of the fractional recovery at outlet a (F_a) with flow rate $\dot{V}(a)$ of a mixture of 2 μm and 9.9 μm polystyrene microspheres in buoyancy-driven mode. The total flow rate ($\dot{V}_{tot}$) through the cell is 0.7 mL min^{-1}. NaCl is added to adjust the carrier density to $\rho_c = 1089.3$ kg m^{-3}. Symbols are defined in Fig. 8.

density is 1138.8 kg m^{-3}, and the viscosity is 0.001508 Pa s (Fig. 11, set (2)). For the fourth set of experiments the carrier density is 1089.3 kg m^{-3}, and the viscosity is 0.001262 Pa s (Fig. 12).

Figure 11 shows that, as the flow rate at outlet b, $\dot{V}(b)$, increases, the fraction of 2.0 μm diameter beads recovered at outlet a decreases. Here, both sets of calculated theoretical data are nearly identical, and thus only one set is presented in the figure. As $\dot{V}(b)$ increases, $\dot{V}(b')$ correspondingly decreases. The volumetric flow rate of the transport region therefore decreases according to Eq. 19, and so the fractional recovery at outlet a decreases according to Eq. 23. Successful separation is evident in Fig. 11, for $\dot{V}(b) > 0.38$ mL min^{-1}. Here, the 9.9 μm beads, with their greater flotation velocity, are mostly directed to outlet a, since F_a, the fraction of beads recovered at outlet a, is close to one. This is because Eq. 4 shows that U, the flotation velocity of the 9.9 μm beads, is large due to the large density difference between the beads and the carrier. Equation 22 then indicates that the volumetric flow rate of the lamina crossed by the particles is similarly large, for all flow rates. Hence, for all obtainable values of $\dot{V}(t)$, the volumetric flow rate of the transport region, the predicted F_a for the 9.9 μm beads is 1. Meanwhile, Fig. 11 also shows that the 2 μm beads are mostly directed to outlet b, since F_a, the fraction of beads directed to outlet a, is close to zero. This is consistent with Eq. 24. Because most of the 9.9 μm beads are directed to one outlet, and most of the 2 μm beads towards the other, successful separation is achieved.

Buoyancy-Driven Separation of Particles, Carrier Density of 1089.3 Kg M^{-3}

The data for the fourth set of experiments are presented in Fig. 12, and are obtained using a carrier density of 1089.3 kg m^{-3}. This figure shows that very good separation with the buoyant mode is obtained for flow rates $\dot{V}(b)$ from 0.40 mL min^{-1} to 0.60 mL min^{-1}. Here, F_a is close to 1 for the 9.9 μm beads, but close to 0 for the 2 μm beads. This means that the majority of the 9.9 μm beads are recovered at outlet a whereas, according to Eqn. 24, most of the 2 μm beads are collected at outlet b, which illustrates excellent separation. These experimental data match theoretical predictions well for the entire range of conditions examined. The lower carrier density in these experiments, compared to the results in Fig. 11, means that the difference in density between the beads and the carrier is smaller. Thus, flotation velocities of the beads U are less negative, and Eqn. 22 shows that the volumetric flow rate of the lamina crossed by the beads is smaller. Thus, according to Eq. 23, theoretical values of F_a are smaller for a given particle at the same flow rate, when compared to situations with higher carrier densities.

From Figs. 11 and 12, it is evident that measured F_a data vary with $\dot{V}(b)$ in a non-linear fashion, noting that the total flow rate $\dot{V}_{tot}$ is maintained constant as these data are acquired. Such non-linearity is consistent with the theory for buoyancy-induced fractionation, which is illustrated by combining Eqs. 22, 23, and 27 to give

$$F_a = \frac{\left[-\frac{bL(\rho_p-\rho_c)gd^2}{18\eta}\right] - \dot{V}(b)}{\dot{V}_{tot} - \dot{V}(b)} + 1 \qquad (32)$$

According to this equation and the associated experimental data in Figs. 11 and 12, non-linear behavior is more pronounced as particle size decreases.

CONCLUSIONS AND SUMMARY

The successful development and application of the new buoyancy-driven mode of Continuous SPLITT Fractionation is demonstrated. The capabilities of the system are illustrated by separating polymer microspheres under a variety of experimental conditions. In all cases, the performance of the new system is satisfactory, and the results obtained are in

agreement with buoyancy-driven SPLITT theory. With this arrangement, the weight of the displaced carrier fluid (and hence the buoyancy force acting on the particle) is greater than the weight of the particle. The net force acting on the particle is therefore upwards and so the particle moves towards the upper wall of the SPLITT Fractionation cell.

Experimentally-measured fractionation results are presented for different magnitudes of carrier density for both the gravitational and buoyancy-driven modes of SPLITT separation. Also presented are variations of experimentally-measured F_a, the factional recovery at outlet a, is given as it varies with $\dot{V}(b)$, the volumetric flow rate at outlet b, with the buoyancy-driven mode of SPLITT cell operation. These data are provided for a carrier density of 1133.9 to 1138.8 kg m^{-3}, and for a carrier density of 1089.3 kg m^{-3}, for fluorescent polymer microspheres of 2.0 μm and 9.9 μm diameter. In all cases, the results are in excellent agreement with theoretical predictions, and show that both the new buoyancy-driven theory and the conventional gravitational theory are applicable to a range of experimental conditions. The sedimentation results also provide qualification of channel performance, which verifies both the experimental procedures, and the channel design and construction.

The new buoyancy-driven mode of SPLITT Fractionation offers theoretical advantages over gravitational sedimentation separations in a number of situations. For example, separations difficult with gravity-driven separation, but easier with buoyancy-driven separation are those where small but dense particles are separated from large, less dense particles, or when the carrier fluid of choice (say, a complex biological buffer) is denser than the particles it carries (cells, for example). A further example of a separation which is more efficient in a buoyancy-driven system is the one step separation of the large particles from a mixture of large particles, smaller particles of the same density, and denser impurities, which would require two separation steps using gravitational SPLITT separation. The results of this fundamental research into a new method of SPLITT fractionation thus gives users of SPLITT cells another effective method to accomplish successful separations.

ACKNOWLEDGEMENTS

The authors acknowledge discussions with Professor Peter Dobson. Prior development efforts by Dr. Helen Townley and Ms. Emilie Holland are also acknowledged. Funding for the effort is provided by the John Fell Fund and the ISIS-UCSF Fund

GLOSSARY

Symbols	
a	top outlet of the channel
a′	top inlet of the channel
b	channel breadth
b	bottom outlet of the channel
b′	bottom inlet of the channel
d	particle diameter
F_a	fractional recovery at outlet a
F_b	fractional recovery at outlet b
F_d	frictional (drag) force acting on the particle
F_g	gravitational force acting on the particle
G	acceleration due to gravity
L	length of channel
R	particle radius
u	velocity of particle relative to fluid
U	sedimentation velocity
V	particle volume
v	streamwise velocity of flow in channel
$\Delta\dot{V}$	volumetric flow rate of the lamina across which the particle sediments
$\dot{V}(a)$	volumetric flow rate at outlet a
$\dot{V}(a')$	volumetric flow rate at inlet a′
$\dot{V}(b)$	volumetric flow rate at outlet b
$\dot{V}(b')$	volumetric flow rate at inlet b′
$\dot{V}(t)$	volumetric flow rate of the transport region
$\dot{V}_{tot}$	total volumetric flow rate through the cell
w	channel thickness
x	axis pointing along length of channel
z	axis pointing along width of channel
η	carrier viscosity
$\Delta\rho$	difference in density between the particle and the carrier fluid
ρ_c	carrier density
ρ_p	particle density

Abbreviations	
bead	fluorescent polymer microsphere
Cat #	catalog number
ISP	inlet splitting plane
OSP	outlet splitting plane
SPLITT	Split-Flow Lateral-Transport Thin

REFERENCES

1. Gupta, S.; Ligrani, P.M.; Myers, M.N.; Giddings, J.C. (1997) Resolution Deterioration and Optimal Operating Conditions in Centrifugal SPLITT Fractionation. Part I: Stable Density Gradients. *J. Micro. Sep.*, *9* (3): 213.
2. Fuh, C.B.; Myers, M.N.; Giddings, J.C. (1992) Analytical SPLITT Fractionation: Rapid Particle Size Analysis and Measurement of Oversized Particles. *Anal. Chem.*, *64* (24): 3125.
3. Fuh, C.B.; Trujillo, E.M.; Giddings, J.C. (1995) Hydrodynamic Characterization of SPLITT Fractionation Cells. *Sep. Sci. Technol.*, *30* (20): 3861.
4. Keil, R.G.; Tsamakis, E.; Fuh, C.B.; Giddings, J.C.; Hedges, J.I. (1994) Mineralogical and textural controls on the organic composition of coastal marine sediments: Hydrodynamic separation using SPLITT-fractionation. *Geochimica et Cosmochimica Acta*, *58* (2): 879.
5. Fuh, C.B.; Giddings, J.C. (1995) Isolation of Human Blood Cells, Platelets, and Plasma Proteins by Centrifugal SPLITT Fractionation. *Biotechnol. Prog.*, *11* (1): 14.
6. Benincasa, M.-A.; Moore, L.R.; Williams, P.S.; Poptic, E.; Carpino, F.; Zborowski, M. (2005) Cell Sorting by One Gravity SPLITT Fractionation. *Anal. Chem.*, *77* (16): 5294.
7. Fuh, C.B.; Myers, M.N.; Giddings, J.C. (1994) Centrifugal SPLITT Fractionation: New Technique for Separation of Colloidal Particles. *Ind. Eng. Chem. Res.*, *33* (2): 355.
8. Giddings, J.C. (1985) A System Based on Split-Flow Lateral-Transport Thin (SPLITT) Separation Cells for Rapid and Continuous Particle Fractionation. *Sep. Sci. Technol.*, *20* (9 & 10): 749.
9. Springston, S.R.; Myers, M.N.; Giddings, J.C. (1987) Continuous Particle Fractionation Based on Gravitational Sedimentation in Split-Flow Thin Cells. *Anal. Chem.*, *59* (2): 344.
10. Giddings, J.C. (1992) Optimization of Transport-Driven Continuous SPLITT Fractionation. *Sep. Sci. Technol.*, *27* (11): 1489.
11. Gupta, S.; Ligrani, P.M.; Giddings, J.C. (1997) Investigations of Performance Characteristics Including Limitations Due to Flow Instabilities in Continuous SPLITT Fractionation. *Sep. Sci. Technol.*, *32* (10): 1629.
12. Lide, D.R. (2008) *CRC Handbook of Chemistry and Physics*, 89th Ed.; Taylor & Francis Group, London, UK.